JGR Oceans

RESEARCH ARTICLE
10.1029/2021JC017352

Special Section:
Uncovering the hidden links between dynamics, chemical, biogeochemical and biological processes under the changing Arctic

The Transpolar Drift Influence on the Arctic Ocean Silicon Cycle

Bianca T. P. Liguori[1], Claudia Ehlert[1], Eva-Maria Nöthig[2], Jan C. van Ooijen[3], and Katharina Pahnke[1]

[1]Marine Isotope Geochemistry, Institute for Chemistry and Biology of the Marine Environment (ICBM), University of Oldenburg, Oldenburg, Germany, [2]Alfred Wegener Institute Helmholtz Centre for Polar and Marine Research, Bremerhaven, Germany, [3]NIOZ Royal Netherlands Institute for Sea Research, Department of Ocean Science (OCS), University of Utrecht, Utrecht, The Netherlands

Abstract During most of the year, diatom production in the ice-covered Central Arctic Ocean (CAO) is limited by light availability and nutrient supply. Therefore, biological production is thought to be generally low, with higher biological production at the sea ice edge and over partially ice-free shelf areas. The major surface ocean current in the CAO is the Transpolar Drift (TPD), which transports sea ice and water from the rivers and shelves of the Laptev and the East Siberian Seas across the CAO toward the Fram Strait, carrying high amounts of terrestrial-derived material over long distances. We used Si isotopes (δ^{30}Si) to better understand the difference between lower and higher biological production areas and how the TPD potentially affects the Si cycle in the CAO. Our data show low dissolved Si concentrations ([DSi]) paired with high values of δ^{30}Si-DSi in all surface samples indicating fractionation by diatoms. Specifically, outside the TPD influence, all nutrients were depleted and supply was limited due to stratified conditions, thus preventing further phytoplankton growth in the area during the sampling time in late summer-early fall. In contrast, under the TPD influence, diatom primary production was limited by low nitrate and strongly limited by light due to the presence of sea ice, even though [DSi] values were much higher than outside the TPD. Based on δ^{30}Si, we could identify low but measurable DSi utilization in the TPD, potentially highlighting the importance of sea ice-attached diatoms transported to the CAO via the TPD for the Si cycle in this region.

Plain Language Summary The growth of siliceous microalgae (diatoms) in the ice-covered Central Arctic Ocean (CAO) can be limited by light and nutrient availability. Due to the limiting conditions, diatom growth is considered to be generally low, with highest growth rates at the sea ice edge and over partially ice-free coastal areas. The major surface water current in the CAO is the Transpolar Drift (TPD), carrying ice and water from rivers and coastal areas across the CAO to the major outflow area, the Fram Strait. We used silicon isotopes to better understand how the TPD potentially influences the silicon cycle in the CAO. Our data show that diatom growth was taking place in all areas studied here, despite different growth limiting factors outside and under the TPD influence. In the area outside the TPD influence, nutrient availability was very low and its supply was limited, which prevented further diatom growth. Under the TPD influence, even with additional nutrient supply from the TPD, only low diatom growth was observed, most likely limited by light availability.

Key Points:

- Primary production and silicon utilization outside the Transpolar Drift are higher than under its influence due to more light availability
- Primary production and lateral water transport under the Transpolar Drift influence were identified from silicon isotope composition
- The Transpolar Drift delivers high dissolved silicon to the surface Arctic Ocean, a unique feature not seen in any other open ocean

Supporting Information:

Supporting Information may be found in the online version of this article.

Correspondence to:

B. T. P. Liguori,
bianca.liguori@uni-oldenburg.de

Citation:

Liguori, B. T. P., Ehlert, C., Nöthig, E.-M., van Ooijen, J. C., & Pahnke, K. (2021). The Transpolar Drift influence on the Arctic Ocean silicon cycle. *Journal of Geophysical Research: Oceans*, *126*, e2021JC017352. https://doi.org/10.1029/2021JC017352

Received 15 MAR 2021
Accepted 18 OCT 2021

1. Introduction

Diatoms are important primary producers playing a central role in the silicon (Si) and carbon cycles of the ocean (Nelson et al., 1995; Tréguer & De La Rocha, 2013). Diatoms require Si in the form of silicic acid ($Si(OH)_4$, hereafter referred to as dissolved Si = DSi), to build their frustules made of biogenic silica ($bSiO_2$) and are therefore one of the main controllers of the Si cycle in the ocean (Nelson et al., 1995). These primary producers are responsible for 40% of the oceanic carbon fixation contributing significantly to the global carbon pump by exporting $bSiO_2$ and carbon to the ocean floor (Nelson et al., 1995; Romero & Hebbeln, 2003; Tréguer & Pondaven, 2000). During sinking, diatom frustules are more resistant than organic carbon compounds to remineralization and can therefore be preserved on the ocean floor, providing insights into the intensity of primary production in the surface waters in the present (e.g., Sarmiento et al., 2004) and past ocean (e.g., De La Rocha et al., 1998).

In the Central Arctic Ocean (CAO), diatoms live in the snow on top of the sea ice, in small ponds on sea ice, in small brine channels and pockets in sea ice, attached underneath sea ice and/or in the seawater under the sea ice (Arrigo, 2017). Ice-associated algae can be responsible for up to 60% of the primary production in the ice-covered CAO (e.g., Fernández-Méndez et al., 2015; Gosselin et al., 1997). The estimated total annual primary production in the Eurasian basin north of 78°N during summer 2012 was 17 ± 7 Tg C yr^{-1}, however, considering attached sea ice algae, a surplus of 16 Tg C yr^{-1} to annual primary production was observed (Fernández-Méndez et al., 2015), demonstrating the importance of these algae for carbon fixation.

In the ice-covered CAO, diatom production is highly seasonal and mainly limited by factors such as light availability, nutrient supply and water stratification. Depending on the latitude and sea ice retreat, light availability is restricted to a short period of the year (Wassmann & Reigstad, 2011). In addition to the short growth season in the CAO, sea ice and especially snow cover strongly limit light penetration and transmission (Perovich, 2017). As the productive season develops during summer, nutrients such as nitrate (NO_3^-), DSi and iron (Fe) can become the limiting factors for primary production in open water areas, leads and areas covered by thin sea ice without snow (Fernández-Méndez et al., 2015; Rijkenberg et al., 2018; Slagter et al., 2017). Additionally, the strong terrestrial freshwater runoff from Siberian and Canadian rivers combined with melting of sea ice induces pronounced stratification of the surface ocean (Nummelin et al., 2016; Rudels et al., 1991) decreasing the availability of upwelled nutrients and hence primary production (Rudels et al., 1991). Due to the prevalence of these limiting factors, biological production is typically considered to be very low in the ice-covered CAO, with higher production at sea ice edges. However, previous studies have shown the presence of blooms up to 100 km away from the sea-ice edge underneath thin sea ice or ice with several leads that enable enough light to reach the water column (Arrigo et al., 2012; Assmy et al., 2017). In general, an increase in primary production in the hitherto still ice covered CAO is expected to gain significance in the future due to further sea ice reduction (Ardyna et al., 2014; Arrigo et al., 2008) and increase in anthropogenically induced nutrient supply (Lewis et al., 2020). However, the role that diatoms will play and how they will respond to the warming in detail is not known, leaving a gap in our current understanding of future perturbations to the Arctic silicon and carbon cycles.

The major source waters to the Arctic Ocean are: (a) the relatively warm and saline contribution from the Atlantic Ocean; (b) Pacific Ocean waters richer in nutrients and less saline than the Atlantic Water (AW); (c) and river water from Siberia and Canada with high nutrient concentrations and terrestrial material (Jones et al., 2003). The AW enters the Arctic Ocean through the deep Fram Strait and the Barents Sea and circulates counterclockwise through the Eurasian Basin (Figure 1) (Aagaard, 1989). The Pacific Water (PW) enters the Arctic Ocean via the Bering Strait (50 m depth), flows through the Chukchi Sea and Canada Basin and towards the North Atlantic through the Canadian Archipelago and the Fram Strait (Jones et al., 2003). The major surface current in the CAO is the TPD that transports sea ice and water from the shelves of the Laptev Sea and East Siberian Sea across the CAO to the Fram Strait (Charette et al., 2020; Kipp et al., 2018). The TPD therefore represents a unique feature delivering terrestrially-derived constituents to the remote CAO, indicated by elevated trace element concentrations (Charette et al., 2020; Rijkenberg et al., 2018), chromophoric dissolved organic matter (CDOM, Slagter et al., 2017) and radium-228 (Kipp et al., 2018). One of the major contributors to the TPD surface current is the Laptev Sea into which the Lena River delivers large amounts of dissolved and particulate material. This includes high concentrations of dissolved organic nitrogen (0.08–0.245 Tg yr^{-1}) and DSi (0.89–1.64 Tg yr^{-1}) (Dittmar & Kattner, 2003), but also large amounts of trace elements (e.g., Charette et al., 2020; Slagter et al., 2017). River inputs are the main source of dissolved and particulate Si to the Ocean (Tréguer & De La Rocha, 2013). However, despite receiving 10% of the global river runoff, the CAO shows persistently low [DSi] (Codispoti et al., 1991), with little known about the Si cycle in the region.

A powerful tool to better understand the Si cycle is the use of the isotope composition of Si ($\delta^{30}Si$) in seawater and/or opal. Silicon has three stable isotopes with different abundances: ^{28}Si (92.23%), ^{29}Si (4.68%) and ^{30}Si (3.08%). Silicon isotopes are fractionated during uptake by diatoms, with lighter isotopes preferentially consumed, affecting the $\delta^{30}Si$ of their biogenic opal ($bSiO_2$) and the residual seawater DSi. These variations in the $\delta^{30}Si$ of $bSiO_2$ ($\delta^{30}Si$-$bSiO_2$) and of DSi ($\delta^{30}Si$-DSi) can be used to study relative Si utilization in the water column, both in modern (e.g., Varela et al., 2004, 2016) and past oceans (e.g., De La Rocha et al., 1998). The utilization of DSi by diatoms in surface waters and later dissolution of their frustules at

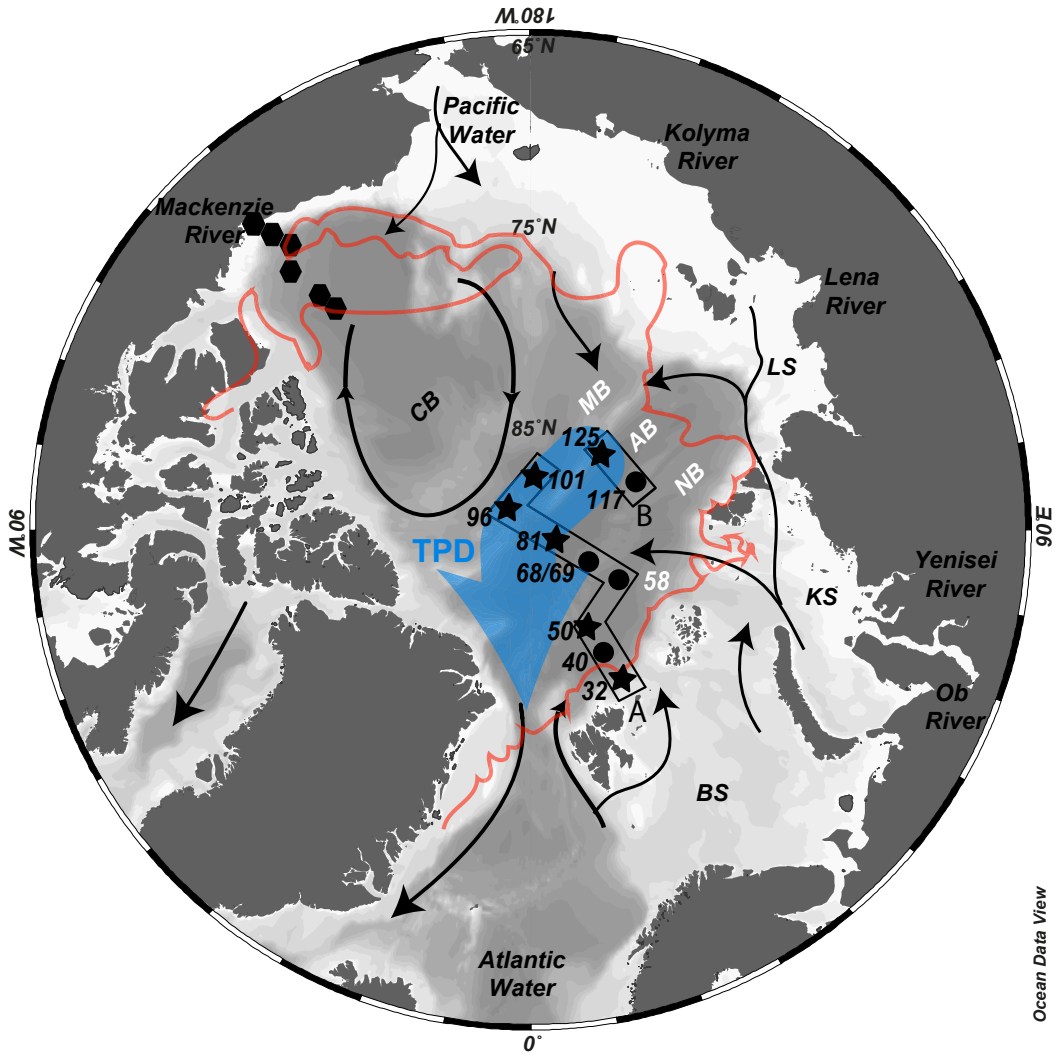

Figure 1. Map of the Arctic Ocean with schematic surface circulations (black arrows). The position of the Transpolar Drift (TPD) is indicated with the broad blue arrow based on chromophoric dissolved organic matter (Slagter et al., 2017). Stations from the present study are numbered: black dots represent samples for δ^{30}Si-DSi; black stars represent samples for δ^{30}Si-DSi and δ^{30}Si-bSiO$_2$; black polygons are the stations from Varela et al. (2016). Thick red line represents the average sea ice extent in August 2015 (National Snow & Ice Data Center database, 2015 - https://nsidc.org). BS, Barents Sea; KS, Kara Sea; LS, Laptev Sea; CB, Canadian Basin; NB, Nansen Basin; AM, Amundsen Basin; MB, Makarov Basin. The figure was produced using Ocean Data View (Schlitzer, 2018) and modified manually.

greater depths control the δ^{30}Si-DSi of seawater (e.g., De La Rocha et al., 2000). Therefore, low [DSi] with higher δ^{30}Si-DSi are typically found in surface waters and high [DSi] with lower δ^{30}Si-DSi are found at greater depths creating an inverse relationship between [DSi] and δ^{30}Si-DSi (e.g., Brzezinski & Jones, 2015; De Souza et al., 2012; Varela et al., 2016). Furthermore, different water masses may carry different Si isotope signatures, allowing us to investigate the mixing and circulation of intermediate and deep water masses using Si isotopes (e.g., Brzezinski & Jones, 2015; De Souza et al., 2012; Liguori, Eherlt, Nöthig, et al., 2020; Liguori, Eherlt, & Pahnke, 2020; Sutton et al., 2018). In a recent study from the same region focusing on the Si cycle in intermediate and deep waters found that surface waters and intermediate/deep waters in the CAO are rather disconnected from each other, mostly due to the fact that particle export from surface waters is limited (Liguori, Eherlt, Nöthig, et al., 2020; Liguori, Eherlt, & Pahnke, 2020).

The aim of this work is to promote a better understanding of the current Si cycle in the surface water of the CAO before greater changes occur due to the fast-changing climate that is affecting the CAO. In particular,

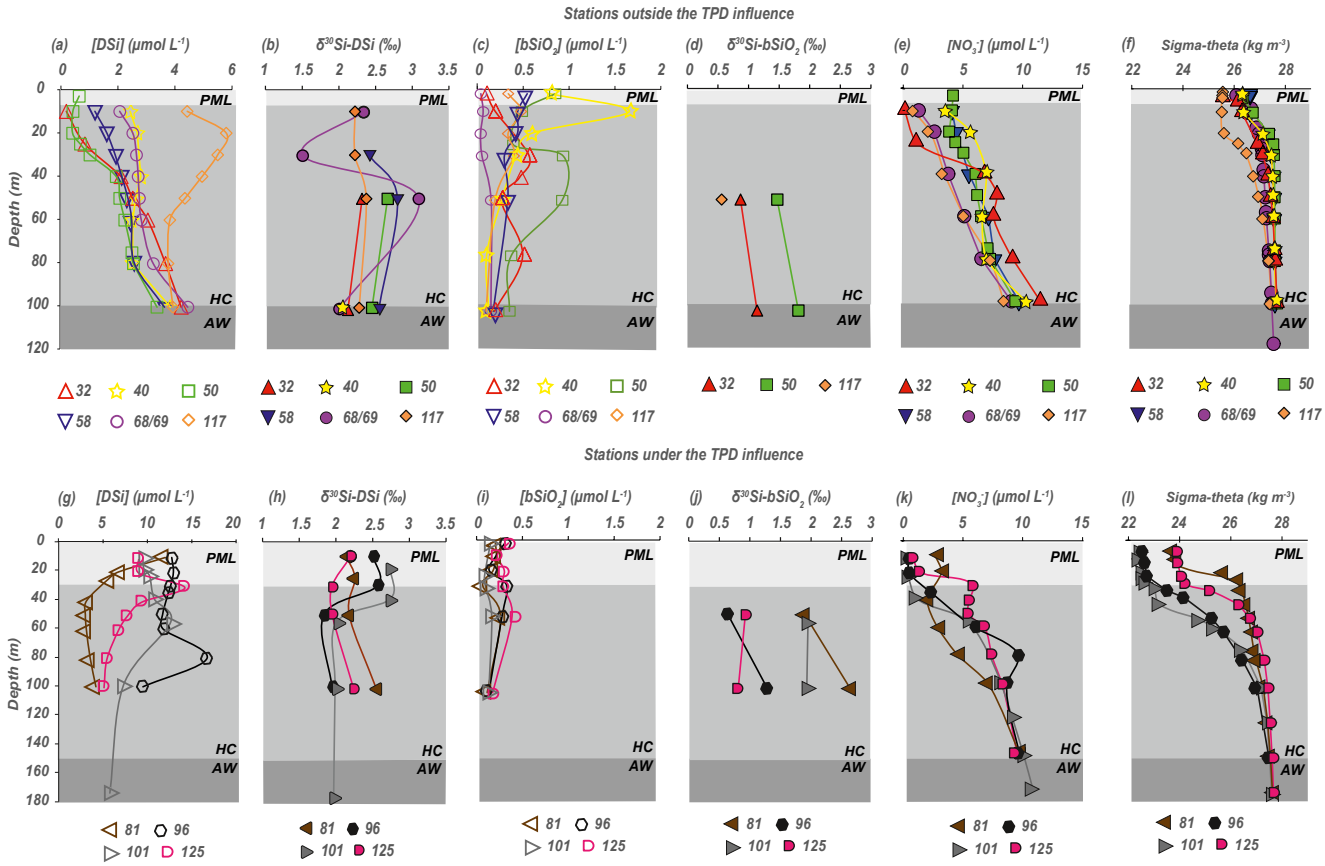

Figure 2. Discrete depth profiles for all stations outside the transpolar drift (TPD) influence (a–f) and under the TPD influence (g–l). (a, g) [DSi] in µmol L^{-1}, (b, h) δ^{30}Si-DSi in ‰, (c, i) [$bSiO_2$] in µmol L^{-1}, (d, j) δ^{30}Si-$bSiO_2$ in ‰, (e, k) [NO_3^-] in µmol L^{-1} and (f, l) sigma-theta in kg m^{-3}. Note the different depth scales for the upper and lower panels. Note the different scales for [DSi]. PML, Polar Mixed Layer; HC, Halocline; AW, Atlantic Water.

the difference between lower and higher primary production areas will be investigated and how the TPD potentially affects the Si cycle in the CAO. We hypothesize that the high nutrient concentrations delivered to the CAO by the TPD influence the nutrient distribution and therefore diatom primary production. We further hypothesize that regions in the CAO under and outside the influence of the TPD are characterized by differences in their respective local Si cycles, which we can detect using Si isotopes. To investigate these hypotheses, we focus on the upper 180 m water depth in the CAO.

2. Material and Methods

2.1. Study Area

Low salinity and temperatures close to the freezing point mark the Polar Mixed Layer (PML) at the surface of the CAO. Below the PML are the pycnocline and the halocline where density and salinity, respectively, increase to the subsurface maximum of the warm AW layer (Rudels et al., 2004). The PML usually extends to around 30 m water depth and occurs at all stations in our study. Outside the TPD influence, the PML is generally shallower and reaches only 10 m water depth. Both the PML and the halocline are thicker under the TPD influence, where the halocline can reach up to 100 m water depth. The PML and halocline receive water from sea ice meltwater, river and PW, all contributing to the low salinity (Rudels et al., 1996). Atlantic Water occurs at 100 m water depth at the stations outside the TPD influence and at 150 m water depth at the TPD influenced stations based on Rudels (2012) (see Figure 2 for reference). In the CAO, the presence of the TDP current is marked by terrestrial input from the Siberian rivers and shelves (e.g., Charette et al., 2020; Krumpen et al., 2019; Rijkenberg et al., 2018). CDOM is a tracer for riverine input (Stedmon et al., 2011). Using this tracer, measured on samples from the same cruise, Slagter et al. (2017) identified the

TPD influence at the following stations and depths covered in our study: stations 81 (at 10 m), 96 (≤50 m), 101 (at 55 m) and 125 (≤30 m) (see Figure 3 for reference). Therefore, we use the same classification for identifying the TPD influence at our stations.

2.2. Sampling

All samples were collected in the framework of the European GEOTRACES program during the TransArc II expedition with the German icebreaker R/V *Polarstern* to the Arctic Ocean (PS94, ARK-XXIX/3, GEOTRACES transect GN04, Tromsø-Bremerhaven) from 17 August to 15 October 2015 (late summer -early fall). This study focuses on the following 10 stations in the CAO depicted in Figure 1: stations 32, 40, 50 and 58 (Nansen Basin), 69 and 117 (Gakkel-Ridge), 81 and 125 (Amundsen Basin) and 96 and 101 (Makarov Basin). All δ^{30}Si data of this study are available online (https://doi.org/10.1594/PANGAEA.920105; Liguori, Eherlt, Nöthig, et al., 2020; Liguori, Eherlt, & Pahnke, 2020).

A standard rosette with 24 × 12 L Niskin bottles equipped with a SeaBird CTD (conductivity, temperature and depth/pressure) system and an oxygen sensor was used to sample for seawater δ^{30}Si-DSi analyses. Around 2 L of water per sample from 10 to 174 m water depth were filtered directly from the Niskin bottles through AcroPak500 filter cartridges (0.8/0.45 μm pore size, Supor® pleated membrane) and stored in acid pre-cleaned (with 0.5 N ultra-clean HCl) Low Density PolyEthylene (LDPE) containers. No further onboard treatment was required.

Samples for [$bSiO_2$] were taken from the CTD using cellulose acetate filters (see Section 2.4 for further details). Suspended particles for particulate δ^{30}Si-$bSiO_2$ analyses were sampled at ~50 and ~100 m water depth at seven stations in the CAO (Figure 1) using in situ pumps (McLane and Challenger) equipped with pre-cleaned (1 N HCl and Milli-Q® water) Supor® filters (0.8 μm pore size, 142 mm diameter). Up to 934 L were pumped through each filter. The filters were cut onboard under a laminar flow hood and a 23 mm diameter piece of each filter (equivalent to ~15 L of pumped seawater) for analyses of δ^{30}Si-$bSiO_2$ was stored folded in a plastic bag in the fridge for later processing in the home laboratory.

2.3. Silicon Concentrations and Pre-Concentration for Dissolved Silicon Isotopes

The [DSi] and other nutrient data used in this study were reported previously by van Ooijen et al. (2016) and are available on PANGAEA (https://doi.org/10.1594/PANGAEA.868396). Seawater samples for δ^{30}Si-DSi analyses (~60 mL each) were treated with a two-step double magnesium hydroxide ($Mg(OH)_2$) coprecipitation method ("MAGIC" method after Karl & Tien, 1992, modified by Liguori, Eherlt, Nöthig, et al., 2020; Liguori, Eherlt, & Pahnke, 2020; Reynolds et al., 2006; De Souza et al., 2012), in order to purify and preconcentrate the DSi. Briefly, this method consist of the double addition of 1% v/v 1M NaOH to seawater samples in two-steps leading to the precipitation of DSi along with $Mg(OH)_2$ due to pH increase with later centrifugation and redissolution in HCl. Sample preparation was done in the clean laboratory of the Institute for Chemistry and Biology of the Marine Environment (ICBM) of the University of Oldenburg, Germany. Only samples with [DSi] >2.14 μmol L^{-1} were processed for Si isotope analyses. The quasi-quantitative Si yield of >97% in the precipitate, especially for very low concentrated samples, was only possible to achieve using an increased settling time of 48 hr for the precipitation step (Liguori, Eherlt, Nöthig, et al., 2020; Liguori, Eherlt, & Pahnke, 2020), different from the previously applied 24 hr proposed by De Souza et al. (2012). This yield is necessary to avoid isotope fractionation due to incomplete coprecipitation with $Mg(OH)_2$ (Reynolds et al., 2006). The yield of the precipitated samples was checked by determining the [DSi] in the supernatant following the method from Hansen and Koroleff (1999).

2.4. Biogenic Silica Concentrations and Isotopes

The particulate $bSiO_2$ concentrations ([$bSiO_2$]) were determined following the method proposed by Bodungen et al. (1991). Briefly, seawater samples (0.35–2 L/sample) collected with Niskin bottles were filtered through cellulose acetate filters (0.8 μm pore size), processed using a wet-alkaline method (with 0.1 M NaOH pretreated 12 hr at 85°C in an oven) and extracted for 2 hr at 85°C in a shaking water bath, and later

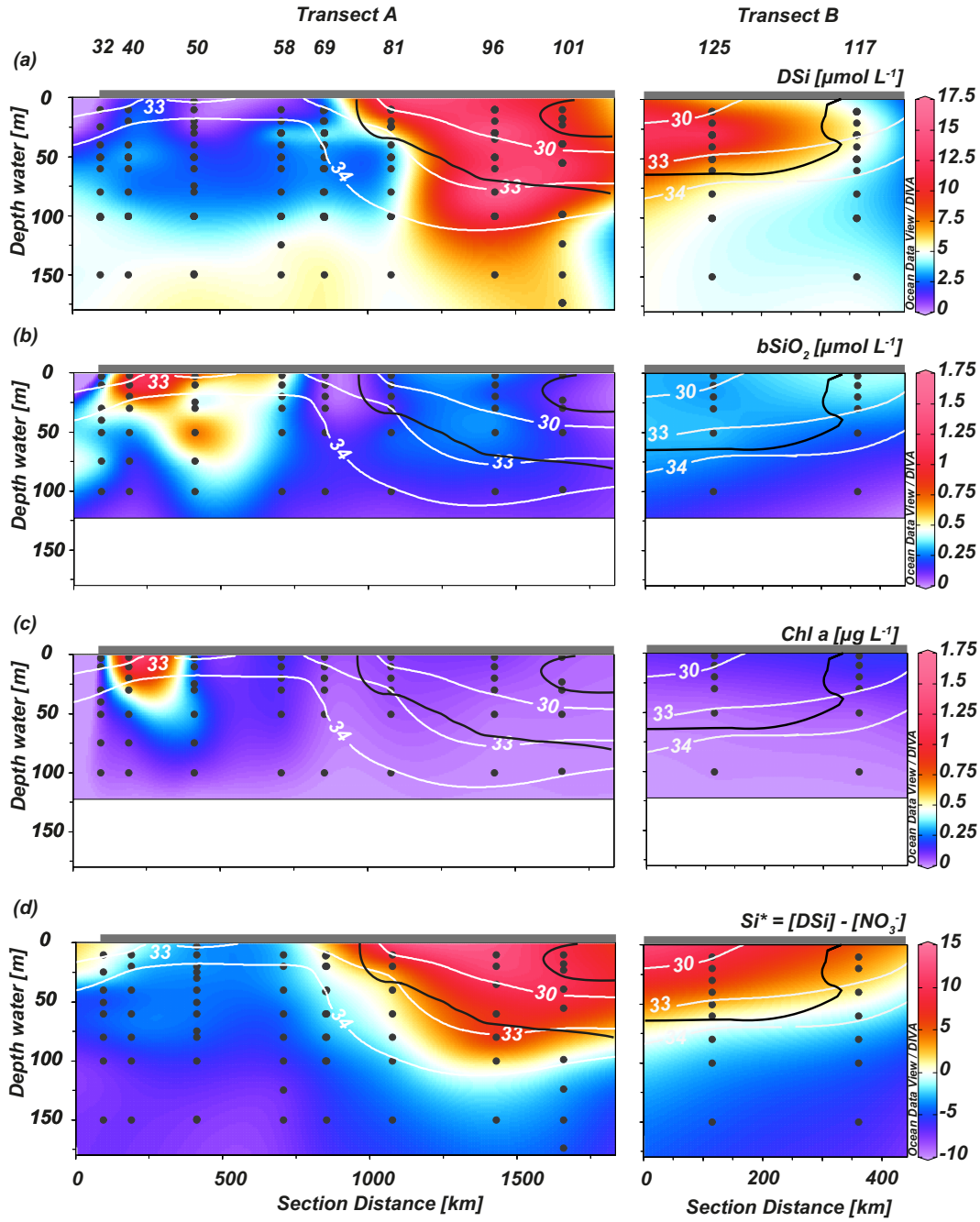

Figure 3. Sections of the surface water to 180 m water depth showing (a) [DSi] (µmol L^{-1}), (b) [$bSiO_2$] (µmol L^{-1}), (c) [Chl *a*] (µg L^{-1}) and (d) Si* = [DSi] – [NO_3^-] (µmol L^{-1}) along the transects shown in Figure 1. Salinity contours are shown in solid white lines. Black dots represent the stations and depths sampled. Solid black lines represent the 0.5 arbitrary unit line for CDOM used by Slagter et al. (2017) to define the TPD boundary and the stations under the TPD influence in the present study. Sea ice distribution is represented by the thick gray line on top of each section. The figure was produced using Ocean Data View (Schlitzer, 2018) and modified manually.

neutralized with 1 N sulfuric acid. Afterward, the [DSi] in the supernatant was determined following the method from Hansen and Koroleff (1999).

The in-situ pump filtered samples for analyses of δ^{30}Si-bSiO$_2$ were dissolved using the NaOH digestion (Ragueneau et al., 2005). The particulate samples were exposed to 0.2 N NaOH for 40 min and later neutralized with 1 N HCl to stop the dissolution. The exposure time of 40 min at 90°C allowed full dissolution of all bSiO$_2$ and minimized the dissolution of lithogenic material. Selected ICP-MS measurements of aluminum concentrations in sample aliquots were all below the detection limit. Assuming the limit of detection representing the maximum contribution of LSi to the samples, we determined a LSi contamination of less than 5% for most samples. Similarly, Varela et al. (2016) estimated only 1%–3% lithogenic contamination during the digestion for similar samples from the Canadian Basin. However, three samples (St. 81,100 m, St. 125,50 m and St. 125,100 m) showed a slightly higher LSi contribution of 7%, 8% and 17%, respectively. By assuming a δ^{30}Si of −0.3‰ of this lithogenic material (Douthitt, 1982), this contamination could have resulted in a shift of the measured δ^{30}Si-bSiO$_2$ of 0.18‰, 0.1‰ and 0.21‰ toward lower values. This is still within the general analytical uncertainty of our measurements (see below). Therefore, due to the low aluminum concentrations in most of the samples, no correction was applied to the δ^{30}Si-bSiO$_2$ values.

2.5. Silicon Isotopes

For Si isotope analyses of seawater and dissolved particles, the Si fraction was isolated from the sample matrix using ion exchange chromatography following the method by Georg et al. (2006) and modified by De Souza et al. (2012).

The Si isotope composition was determined in wet plasma mode on a Neptune Plus™ Multi Collector Inductively Coupled Plasma Mass Spectrometer (MC-ICPMS) (Thermo Fisher Scientific Inc., Germany) at the ICBM, University of Oldenburg. The samples were doped with magnesium (Mg) for mass bias correction (Cardinal et al., 2003; Oelze et al., 2016). Measurements were carried out with the standard-sample bracketing method using the NBS28 quartz sand reference material as standard and by measuring on the left side of the peak shoulder to avoid isobaric interferences for example, of nitrogen ($^{14}N_2$) and nitric oxide ($^{14}N^{16}O$) (see also Ehlert et al., 2016; Grasse et al., 2017). The concentrations used for analysis of seawater samples were ∼0.8 ppm for Si and ∼0.5 ppm for Mg, while particle samples were usually measured at ∼0.5 ppm Si and ∼0.4 ppm Mg due to the limited amount of sample material available. Isotope ratios are expressed relative to the NBS28 using the delta notation (‰):

$$\delta^{x}Si = \left[\frac{(^{x}Si \,/\, ^{28}Si)_{sample}}{(^{x}Si \,/\, ^{28}Si)_{NBS28}} - 1 \right] \times 1000 \quad (1)$$

where ^{x}Si is either ^{29}Si or ^{30}Si.

The data presented here were obtained as δ^{29}Si and converted to δ^{30}Si using a multiplication factor of 1.93 (De La Rocha, 2002) (Figure S1, see Supporting Information S1).

Most of the samples were prepared as full replicates including the MAGIC precipitation step and column chemistry and run in different analytical sessions (n = number of measurements, https://doi.org/10.1594/PANGAEA.920105; Liguori, Eherlt, Nöthig, et al., 2020). External reproducibility is given as "2SD repeated" if true replicates of a water sample were processed with the MAGIC precipitation method and measured on different analytical days, or as "2SD smp brack.", if the sample was precipitated and measured only once (standard deviation resulted from the standard-sample bracketing method). Particle samples were processed and measured only once, except for one sample that could be measured two times on different analytical days.

2.6. Reproducibility of Standards and Seawater Intercalibration Samples

Repeated measurements of reference materials Big Batch and Diatomite were carried out during the time of this study and gave an average δ^{29}Si value of −5.47 ± 0.16‰ and δ^{30}Si value of −10.56 ± 0.31‰ (2SD repeated; n = 58) and an average δ^{29}Si value of 0.59 ± 0.31‰ and δ^{30}Si value of 1.15 ± 0.59‰ (2SD repeated;

$n = 36$), respectively. The values from Big Batch and Diatomite are within the range of published intercalibration results of $\delta^{29}Si = -5.35 \pm 0.30‰$ and $\delta^{30}Si = -10.48 \pm 0.57‰$ and $\delta^{29}Si = 0.64 \pm 0.14‰$ and $\delta^{30}Si = 1.26 \pm 0.20‰$, respectively (2SD, Grasse et al., 2017; Reynolds et al., 2007). In addition, analyses of ALOHA seawater samples from the international GEOTRACES intercalibration study yielded $\delta^{29}Si = 0.81 \pm 0.13‰$ and δ^{30}Si-DSi $= 1.57 \pm 0.25‰$ (2SD repeated; $n = 4$) for $ALOHA_{300}$ (~9 µmol L^{-1} Si) and $\delta^{29}Si = 0.62 \pm 0.22‰$ and δ^{30}Si-DSi $= 1.20 \pm 0.42‰$ (2SD repeated; $n = 5$) for $ALOHA_{1000}$ (~113 µmol L^{-1} Si). These results are within the range of published $ALOHA_{300}$ $\delta^{29}Si$ of $0.87 \pm 0.10‰$ and δ^{30}Si-DSi of $1.68 \pm 0.35‰$ and $ALOHA_{1000}$ $\delta^{29}Si$ of $0.65 \pm 0.10‰$ and δ^{30}Si-DSi of $1.24 \pm 0.20‰$ (Grasse et al., 2017). A section about data quality together with a cross plot for $\delta^{30}Si$ vs. $\delta^{29}Si$ for standards Big Batch and Diatomite along with all samples are presented in the supplementary material and show a linear regression line with a slope of 0.512 ($R^2 = 0.998$, $n = 192$, Figure S1 in Supporting Information S1) (Reynolds et al., 2007).

General offsets between laboratories in intercalibration studies have been demonstrated (Grasse et al., 2017). To address the issues, we refrain from detailed comparisons of absolute data with other published studies in the Arctic Ocean (e.g., Varela et al., 2016) and focus on the general variations within our data set.

2.7. Chlorophyll *a*

Between 1 and 2 L of seawater were filtered through 25-mm diameter GF/F filters (Whatman, Kent, UK) at 5 to 7 depths per station between the surface and 100 m water depth. The filters were stored at −20°C for processing at the home laboratory. Chlorophyll *a* (Chl *a*) was extracted using 90% acetone and measured using a fluorometer (Turner Designs, Sunnyvale, CA, USA) (Edler, 1979; Evans & Anderson, 1987). These data are available in Nöthig et al. (2020) and on PANGAEA (https://doi.org/10.1594/PANGAEA.887934; Nöthig et al., 2018).

3. Results

3.1. Silicon Concentrations and Isotopes

The [DSi] in the upper 10–180 m water depth ranged between 0.2 to 16.7 µmol L^{-1} (Figures 2a, 2g and 3a) and the δ^{30}Si-DSi ranged between 1.5‰ to 3.1‰ (Figures 2b and 2h). For stations 32, 50 and 58, the [DSi] at 10 m water depth was insufficient for δ^{30}Si-DSi analyses. δ^{30}Si-DSi were only determined at 100 m water depth at station 40.

In general, the stations outside the TPD influence (stations 32, 40, 50, 58, 69 and 117; Figures 2a and 2b) show typical vertical profiles of low [DSi] in surface water (10 m water depth) and increasing concentrations with depth (except station 117). The [DSi] at all six stations show a maximum of ~4 µmol L^{-1} with higher values at 100 m (except station 117, where [DSi] is higher compared to other stations and has a subsurface maximum of ~6 µmol L^{-1}). At stations 32 and 50, the δ^{30}Si-DSi is higher at the shallower depths (50 m) and decreases with depth (to 100 m depth). At station 58, the δ^{30}Si-DSi increases toward 50 m and decreases at 100 m again. Station 117 shows only very small variations at all depths with an average value of $2.27 \pm 0.07‰$.

Stations under the TPD influence (stations 81, 96, 101 and 125; Figures 2g and 2h) are generally characterized by higher [DSi] compared to stations outside the TPD influence. These stations show unique [DSi] and δ^{30}Si-DSi profiles that differ from those typically found in the oceans and outside the TPD influence. At station 81, the [DSi] decreases by 7 µmol L^{-1} between the surface layer and 100 m water depth. In contrast, stations 96, 101 and 125 show low [DSi] at the surface, an increase in [DSi] at 80, 55 and 30 m water depth, respectively, and a shift back toward lower [DSi] at ~100 m. The δ^{30}Si-DSi profiles at stations 96 and 101 are generally characterized by a decrease of ~0.7‰ between the surface and 100 m water depth (Figure 2h). Stations 81 and 125 show less variation with water depth with average values of $2.28 \pm 0.18‰$ and $2.08 \pm 0.16‰$, respectively.

3.2. Biogenic Silica Concentrations and Isotopes

The [$bSiO_2$] vary from 0.04 to 1.66 μmol L^{-1} (Figures 2c, 2i and 3b) and δ^{30}Si-$bSiO_2$ range from 0.5‰ to 2.6‰ (Figures 2d and 2j). The higher [$bSiO_2$] are found at shallower depths at stations 40 and 50 outside the TPD and their δ^{30}Si-$bSiO_2$ range between 0.6‰ and 1.76‰. In contrast, the stations under the TPD influence show low [$bSiO_2$] around 0.4 μmol L^{-1} throughout the water column, however, their respective δ^{30}Si-$bSiO_2$ range similarly between 0.6‰ and 2.6‰. At deeper levels, a decrease of [$bSiO_2$] is associated with increased δ^{30}Si-$bSiO_2$ between 50 and 100 m water depth (except at stations 101 and 125).

3.3. Chlorophyll *a* Concentrations

The Chl *a* concentrations ([Chl *a*]) ranged between 0.005 and 1.634 μg L^{-1} (Figure 3c). Higher [Chl *a*] are observed in the upper 50 m in all stations in the study area. Outside the TPD influence, the highest [Chl *a*] are found at the surface at station 40. At this station, high [Chl *a*] extend down to depths of 30 m and decrease toward 100 m. Station 69 has low [Chl *a*] from surface to 100 m. Under the TPD influence, highest surface [Chl *a*] are determined at station 125, yet much lower than outside the TPD influence.

4. Discussion

We investigated whether high nutrient concentrations delivered to the CAO by the TPD could have an influence on the nutrient distribution and therefore on diatom primary production in surface waters. Additionally, we also wanted to understand whether Arctic waters under and outside of the TPD influence can be characterized by differences in their respective local Si cycles. The main sources of nutrients to the surface water of the CAO are: (a) AW inflow, (b) river input (to our study area mainly by Lena, Yenisei and Ob), transported across the CAO in the TPD (Charette et al., 2020; Rijkenberg et al., 2018; Slagter et al., 2017; Paffrath et al., 2021), and (c) PW inflow through the Bering Strait (Figure 1) (Aagaard, 1989). These different sources create specific environmental conditions in separate parts of the CAO. Therefore, we split the study area in two different parts: stations outside the TPD influence (stations 32, 40, 50, 58, 69 and 117) and stations under the TPD influence (stations 81, 96, 101 and 125, according to the definition by Slagter et al., 2017). Accordingly, we will discuss the processes that affect the Si cycle in the surface water by comparing these two areas.

4.1. Regional Differences in Production and Limiting Conditions

The seasonal evolution of phytoplankton blooms in the Arctic Ocean follows ice retreat and light availability (Leu et al., 2011; Randelhoff et al., 2015), with bloom conditions, at the sea ice or in the water column, starting at different months of the year depending on the location and latitude. During winter months, the system shows no/low primary production due to the absence of light while nutrients can be supplied via convective mixing and regeneration of particles before the productive season (e.g., Randelhoff et al., 2015; Uhlig et al., 2019). The present study was carried out during late summer-early fall, therefore the main biomass increase at the sea ice edge as well as pelagic bloom had finished, at least in the Atlantic sector, and nutrient remineralization in the water column is assumed to have already started (Leu et al., 2011; Wassmann & Reigstad, 2011). Strong ice-covered regions under the TPD behaved differently.

4.1.1. Outside the TPD Influence

In the area outside the TPD influence (between 75°N and 85°N) during the sampling time (around September 2015), the phytoplankton community was dominated by diatoms (0–50 m) (Uhlig et al., 2019). Consequently, strongest NO_3^- and DSi depletions coincided with elevated [Chl *a*] and [$bSiO_2$] (Figure 3) representing recent or ongoing phytoplankton growth, as indicated by Uhlig et al. (2019). The low [DSi] in surface waters and the high δ^{30}Si-DSi values compared to the underlying water suggest effective DSi utilization by diatoms in Atlantic influenced waters in the Eurasian Basin (Figures 2a and 2b). This is especially true at the first stations of the transect where the lowest [DSi] were determined (stations 32, 40 and 50). The highest [$bSiO_2$] (~1.6 μmol L^{-1}) was found at the edge of the sea ice at station 40 at 10 m depth (Figure 3b). At the stations 32, 40 and 50, where sea ice cover was 77%, 86% and 93%, respectively (www.nsidc.org) high [Chl *a*] values were restricted to the upper 30 m, most likely due to the stratification in combination with

radiation income (Laney et al., 2017). Elevated [$bSiO_2$] extended down to approximately 100 m, indicating sinking of $bSiO_2$ (Figure 3b) either due to sinking diatoms from the water column or out of melted sea ice. According to Uhlig et al. (2019), most of the phytoplankton was found directly under the sea ice down to 25 m water depth during the cruise, supporting our findings. In the area around the sea ice edge, where light is more abundant, most of the primary production occurs in the pelagic zone and is not associated with sea ice (Fernández-Méndez et al., 2015).

Light or nutrient limitation, either by macronutrients such as phosphorus or NO_3^-, or micronutrients such as Fe, can affect the diatom uptake ratio of DSi:NO_3^- of ~1:1 (Brzezinski, 1985; Brzezinski et al., 2003; Claquin et al., 2002). For example, diatoms show higher DSi:NO_3^- uptake ratios under Fe-limiting conditions (Brzezinski, 1985; Brzezinski et al., 2003). An indicator for the uptake ratio by diatoms is the Si* ([DSi] – [NO_3^-], Figure 3d) value, reflecting the nutrient status in the water column related to the requirements of diatoms (Sarmiento et al., 2004). At the stations outside the TPD influence, values of Si* were negative (except stations 32 and 69 at 10 m water depth and 117 down to 50 m water depth) indicating surplus of NO_3^- compared to [DSi]. At station 32, both nutrients were very low at 10 m water depth indicating total depletion due to primary production. At 69 and 117, where Si* was positive, higher values of [DSi] than [NO_3^-] were determined, potentially indicating less diatom production due to the presence of more sea ice further in the CAO leading to light limitation (Figures 2a and 2e). The low δ^{30}Si-DSi variation at station 117 is in line with low diatom production.

In general, the dominant sources of Fe to the stations outside the TPD are sea ice melt, dust input and supply from AW (Rijkenberg et al., 2018). Iron concentrations in the upper 100 m outside the TPD influence, measured on the same cruise, were very low (0.03–0.21 nM), and Fe was limiting throughout the Nansen Basin surface waters (Rijkenberg et al., 2018). The distribution of Fe concentrations is very similar to the distribution of [DSi], in line with co-limitation of both nutrients restricting diatom growth in the Nansen Basin, as suggested previously by Rijkenberg et al. (2018). The higher [NO_3^-] than [DSi] (and negative Si*) determined at the other stations outside the TPD influence can be due to Fe limitation that leads to a higher uptake of DSi relative to NO_3^-. In consequence, the increased uptake ratio of DSi:NO_3^- by diatoms under Fe limitation (Brzezinski et al., 2003) would lead to stronger DSi depletion compared to NO_3^-.

4.1.2. Under the TPD Influence

During the sampling time (around September 2015), the phytoplankton community in the upper 50 m was dominated by diatoms and chlorophytes (Uhlig et al., 2019). Although present, phytoplankton production was low in the CAO during sampling time (Uhlig et al., 2019). Lower [$bSiO_2$] and [Chl *a*] were measured at stations influenced by the TPD compared to stations outside the TPD influence (Figures 3b and 3c). Additionally, the stations under the TPD influence were characterized by higher [DSi] in surface waters than outside the TPD, but comparable δ^{30}Si-DSi (Figures 2g, 2h and 3a) were found at stations under and outside the TPD influence. The latter is pointing toward Si uptake implying an influence of pelagic or sea ice attached diatoms at these stations. This is confirmed by pigment determination (high ratio of fucoxanthin to Chl *a*) completed by Uhlig et al. (2019). Sea ice diatoms and sea ice attached diatoms can use the water below for nutrient uptake. For example, *Nitzschia frigida* or *Melosira arctica,* species that live attached to the underside of sea ice, are widespread in the CAO and are also found as dominant species in sediment traps deployed under sea ice in the CAO (Boetius et al., 2013; Fernández-Méndez et al., 2015; Lalande et al., 2019; Poulin et al., 2014; Zernova et al., 2000). *M. arctica* grows meter-long filaments reaching down into the water column therefore increasing its chances to take up nutrients from the underlying water (Fernández-Méndez et al., 2014, 2015). Such diatoms travel with the TPD attached to the underside of sea ice from the shelves to the CAO (Fernández-Méndez et al., 2015; Lalande et al., 2014, 2019). The presence of those species could explain the lower [DSi] and higher δ^{30}Si-DSi in surface water compared to subsurface due to ongoing growth but would be underestimated in the [$bSiO_2$] and [Chl *a*] as they would not have been sampled or detected in the water column. Samples for Chl *a* and $bSiO_2$ determination were taken only from the water column with Niskin bottles, therefore missing some diatom populations, such as sea ice attached algae like *M. arctica* (Pomeroy, 1997). In a study using sediment traps attached to the drifting sea ice at 2–25 m in the same region as this study, Lalande et al. (2014) found *M. arctica* at most of the stations in the CAO suggesting that this diatom could also have been present in the area during the sampling time for our study.

The stations under the TPD influence showed [DSi] and δ^{30}Si-DSi profiles following a unique pattern, in which moderate [DSi] and high δ^{30}Si-DSi were present at the surface and high [DSi] and lower δ^{30}Si-DSi occurred near ~50 m followed again by a slight decrease in [DSi] and downward increase in δ^{30}Si-DSi (exception station 81, Figures 2g, 2h and 3a). This is indicative of DSi utilization and fractionation by diatoms in the surface water, for example, pelagic or sea ice assemblages, leaving the surface water isotopically heavier (De La Rocha et al., 1997, 2000). The influence of diatoms usually overprints any signal from water mass mixing in the shallow ocean (Brzezinski & Jones, 2015; De Souza et al., 2012). Yet, at subsurface depths within the TPD flow path, lower δ^{30}Si-DSi and elevated [DSi] are present around 30–50 m water depth. Two scenarios could explain the observed low δ^{30}Si-DSi and high [DSi] in subsurface waters: (a) diatom remineralization and (b) lateral transport of waters with lower δ^{30}Si-DSi and higher [DSi]. The first scenario could lead to the vertical decrease in δ^{30}Si-DSi and increase in [DSi] due to remineralization and further dissolution of sinking $bSiO_2$ that would release its lighter isotopes to the water, therefore lowering the ambient δ^{30}Si-DSi and increasing the [DSi] (Demarest et al., 2009). However, the apparent scarcity of primary producers together with very low [$bSiO_2$] and a photic zone <50 m in the CAO (Laney et al., 2017) render this scenario unlikely. The second scenario could indicate that at around 30–50 m water depth high [DSi] and lighter δ^{30}Si-DSi signatures are due to lateral transport of waters from the shelves within the TPD. Pacific water (δ^{30}Si-DSi of ~1‰, Reynolds et al., 2006) and waters from Lena (δ^{30}Si-DSi of ~1.45‰, Engström, 2009) and Yenisey (δ^{30}Si-DSi of ~1.6‰, Mavromatis et al., 2016) rivers contribute to shelf waters being deliveried to the CAO by the TPD with high [DSi] and terrestrial δ^{30}Si-DSi signature. Varela et al. (2016) determined a minimum in δ^{30}Si-DSi at depths between 125 and 250 m (deeper than the present study) in the Canadian Basin and attributed such shift to modified PW influence (δ^{30}Si-DSi of 1.84 ± 0.10‰). However, Paffrath et al. (2021) using neodymium isotopes, from samples of the same cruise as presented here, determined no PW influence in the area in line with PW being restricted to the Canadian Basin. High river contribution is seen in the top 50–100 m of the water column for other tracers such as Fe (Rijkenberg et al., 2018; Slagter et al., 2017), radium (Rutgers van der Loeff et al., 2018), rare earth elements (Paffrath et al., 2021) and many other trace elements (Charette et al., 2020). In addition, a recent study also showed the influence of meteoric water in the TPD highlighting both high [DSi] and an increase in δ^{30}Si-DSi from an annual average river input of ~1.3‰ (previously determined by Sun et al., 2018) to an average of 2.29‰ within the TPD, implying modification of river water by biological activity across the shelves (Brzezinski et al., 2021). Therefore, an in-depth understanding of the Si cycle over the shelves in the Arctic Ocean and the modifications caused in river waters crossing these areas is necessary for a more comprehensive picture of the Si cycle in the CAO and its influence on the global ocean. At depths >100 m, the δ^{30}Si-DSi is similar to the stations outside the TPD influence with values around 2.14 ± 0.26‰ (Figure 2h), indicating the basin wide influence of the AW (AW endmember defined from the average δ^{30}Si-DSi at 100 m from all stations outside the TPD, δ^{30}Si-DSi = 2.24 ± 0.22‰, see Section 4.2.1 below).

The conditions at the stations under the TPD influence suggest that nutrients, for example, DSi and Fe, from the TPD sustain the low, but still present primary production in the CAO. In contrast to stations outside the TPD influence, [DSi] under the TPD influence is not fully depleted (>3 μmol L^{-1}). The higher [DSi] determined in waters under the TPD influence is in contrast to the upper water column in most regions, where DSi is rapidly utilized by diatoms under optimal conditions. Consequently, the Si* in the area shows positive values (Figure 3d), indicating that diatoms are not limited by DSi availability. Overall, [NO_3^-] was very low, except at station 81, indicating NO_3^- limiting conditions (Figure 2k). Despite the low [NO_3^-], diatoms can outcompete other phytoplankton for NO_3^- due to their capability of taking it up at very low ambient concentrations (Lewis et al., 2019). Thus, the presence of diatoms depleting the [DSi] and [NO_3^-] and increasing the δ^{30}Si-DSi can explain the observed features. Additionally, no limitation of Fe was found at the stations under the TPD influence due to the TPD supplying high amounts of dissolved Fe from the shelves (Rijkenberg et al., 2018). Besides nutrients, light availability is also an important factor affecting primary producers (e.g., diatoms) in the CAO that must be considered. According to Laney et al. (2017), light is available for primary producers under ~1 m sea ice down to ~20–40 m water depth. During the sampling time, the average sea ice plus snow thickness obtained at all stations during the survey was 1.60 ± 0.65 m (Schauer, 2016). Therefore, pelagic primary producers, including diatoms, were limited by NO_3^- and light availability at the stations under the TPD, due to pack sea ice covered by snow limiting light penetration.

4.2. Estimation of Fractionation Behavior of Diatoms

Two simple models are often used to estimate the Si fractionation behavior by diatoms during biological uptake and the nutrient supply status for diatoms: (a) the closed system or Rayleigh model that assumes nutrient consumption and isotope fractionation in a closed system after a single input of nutrients, and (b) the open or steady state system model assuming that there is a continuous supply of DSi and partial consumption (see Supporting Information S1 for further information). In order to estimate the biological fractionation in surface waters with the open and closed system models, we used depths ≤50 m for stations outside the TPD influence and <50 m for stations under the TPD influence based on the depth of the photic zone (Laney et al., 2017). Unfortunately, at stations 32, 40 and 50 we could not determine δ^{30}Si-DSi from <50 m water depth (see Section 3.1), therefore these referred depths were excluded from the model. In both areas, the calculated $^{30}\varepsilon$ from both models indicate no fractionation between diatoms and seawater during DSi utilization (Figure S2 in Supporting Information S1). The values are unrealistic, showing no correlation and do not agree with the average literature value for $^{30}\varepsilon$ of −1.1‰ (e.g., De La Rocha et al., 1997; Sutton et al., 2013), highlighting the limitations in using such simple models in the CAO.

Based on the local environmental conditions, an open or semi-closed system would be more suitable to describe nutrient supply and utilization behavior at the stations outside the TPD. This is because the AW inflow and melting of sea ice at the sea ice edge can re-supply nutrients due to induced convection down to the halocline during sea ice formation (Rudels et al., 1991; Uhlig et al., 2019). Under the TPD, it is expected that a semi-closed system would be more suitable because a parcel of water, with an initially high nutrient content, is transported laterally from the shelf toward the CAO allowing for increased utilization of nutrients along its flowpath. Due to the strong halocline, upward mixing, which could replenish the nutrient stock, is reduced (e.g., Uhlig et al., 2019).

The calculation of utilization and fractionation with both models depends on good estimates of source water [DSi] and δ^{30}Si composition prior to any biological influence in the area to be studied (Cardinal et al., 2005). Therefore, our source water composition estimates and resulting $^{30}\varepsilon$ calculations could change with more precise knowledge of the water mass endmember δ^{30}Si-DSi. Most importantly, the chosen endmembers are based on studies that determined the δ^{30}Si of waters that did not cross the extensive shelf areas in the Arctic Ocean. This, however, most likely would have a huge impact on the δ^{30}Si-DSi composition as the shelves are the most productive areas in this ocean.

In addition, three factors could have played a role in influencing the behavior of the models and description of the system in our study. First, the strong depletion of DSi in many surface waters (10 m) made it impossible to analyze their δ^{30}Si-DSi resulting in a partly scattered data set, which complicates interpretation of the models. Second, we do have only a broad overview of which primary producers were dominant at which time in our study, that is, diatoms vs. non-diatoms. However, discrete samples as well as regions in the CAO might be characterized by different diatom species assemblages. This could cause differences in species-dependent fractionation behavior (Sutton et al., 2013) for the pelagic diatoms in general, which are more likely to grow in an open system. In addition, this could be amplified by variable relative population contributions from sea ice diatoms (Fripiat et al., 2007), which are more likely to grow in a closed system. Third, the time of sampling during late summer (August–October), that is, after the spring bloom period, reflects a mixture of ongoing nutrient utilization and remineralization signals in the water column, which both have an effect on the measured δ^{30}Si-DSi. Additionally, the strong stratification in the water column preventing particles export below the mixed layer (Liguori, Eherlt, Nöthig, et al., 2020; Liguori, Eherlt, & Pahnke, 2020) reinforces this third assumption.

4.3. Future Implications on the Si Biogeochemistry Due To Climate Change

The Arctic Ocean has been changing faster than any other ocean over the past decades (IPCC, 2014). The increase in temperature has led to thawing of permafrost around the Arctic (Schuur & Mack, 2018), a decrease in thickness and permanence of the sea ice (Stroeve et al., 2018) and an increase in warm-nutrient-poor AW entering the Arctic Ocean, the "Atlantification", leading to further loss of sea ice thickness (Polyakov et al., 2017). And most recently, Lewis et al. (2020) suggested that these changes, associated with anthropogenic climate change, have led to a larger supply of new nutrients to the entire Arctic Ocean,

which increased the phytoplankton concentrations, therefore primary production. All of these aspects can potentially modify the marine ecosystem and the Si cycle in particular.

The present study has shown that at stations outside the TPD influence, where light limitation is lower compared to the stations under the TPD influence, high [Chl *a*] and [$bSiO_2$] together with persistently low [DSi] and high δ^{30}Si-DSi at the surface indicate diatom production. In contrast, at stations under the TPD influence in the CAO, elevated [DSi] and light δ^{30}Si-DSi are found at subsurface depths far into the open CAO, a feature not observed in any other ocean and interpreted as lateral transport of terrestrial and shelf signals by the TPD. This is in agreement with previous findings showing high influence of terrestrial material (e.g., Charette et al., 2020; Rijkenberg et al., 2018). Both areas differ concerning the supply of macro- and micronutrients. Outside the TPD nutrient concentrations are low, with DSi and Fe limitation, with the opposite true for stations under the TPD influence, where NO_3^- and light are limiting.

Due to the fast-changing conditions in the Arctic Ocean, the current situation is likely to change. In areas outside the TPD, an increase in nutrient-poor AW inflow to the Arctic Ocean is expected to deliver less [DSi]. This is because a decrease in [DSi] has been found in the subpolar North Atlantic due to a shallower winter mixing there over the past 25 years (Hátún et al., 2017). These changes in the [DSi] in the subpolar region will significantly impact diatom production and may decrease the duration of the summer bloom, with a possible shift in community composition from diatoms to non-silicified phytoplankton, and consequently with changes to the biological carbon pump (e.g., Hátún et al., 2017). Such conditions could potentially influence the whole CAO Si cycle due to the "Atlantification" of the Arctic Ocean (Polyakov et al., 2017).

Contrarily, in the area under the TPD influence, an increase in DSi is expected in the future due to an increase in supply by rivers. This is because an 7% increase in river discharge has been observed since 1930 (start of monitoring, Peterson et al., 2002). This might lead to an increase in [DSi] supply to the TPD as rivers are the main source of Si to the oceans (Tréguer & De La Rocha, 2013). Additionally, it has been shown that with the permafrost thawing, an increase in weathering, and therefore an increase in [DSi] in rivers could occur during summer (Pokrovsky et al., 2013). An increase in PW inflow through the Bering Strait by 50% was found which can influence the nutrient delivery to the Arctic Ocean (Woodgate, 2018). Additionally, light availability is also expected to increase due to sea ice loss. Arrigo and van Dijken (2015) reported an increase in primary production by ~30% due to higher light availability for primary producers in response to sea ice loss. A continuing decrease in CAO sea ice cover would therefore be expected to foster primary production. Futhermore, it was shown that with the ongoing thinning of sea ice, less ice-rafted material reaches Fram Strait due to early melting of the sea, which can increase light availability due to less sediment-landen sea ice-so called dirty ice (Krumpen et al., 2019). The lack of sea ice could also change the ecosystem in terms of habitat, from attached sea ice to pelagial diatoms, and communities living in the CAO (Arrigo et al., 2010). Some diatoms, such as *M. arctica*, can form huge filaments under the sea ice and travel attached to the ice. Without the sea ice, such communities would lose their habitat with implications for the CAO food web and carbon pump (Boetius et al., 2013). The use of δ^{30}Si-DSi in the present study has shown that these communities are likely present in the study area, shifting the δ^{30}Si-DSi of surface waters and highlighting the importance of the TPD in delivering DSi to the CAO. Therefore, an increase in nutrient delivery and light availability in the area has the potential to increase DSi consumption and BSi production. Currently, the limiting variables in the CAO, under the TPD influence, are light and NO_3^-, but with the lack of sea ice during summer a greater effect of wind force may additionally foster primary production due to upward mixing of nutrients (Zhang et al., 2004), changing the entire Si cycle in the area.

5. Conclusions

We here presented δ^{30}Si-DSi and δ^{30}Si-$bSiO_2$ values for the CAO upper water column (<180 m) along GEOTRACES transect GN04 from the Eurasian Basin to the Makarov Basin. Values of δ^{30}Si-DSi were high in all shallow samples indicating fractionation during DSi utilization by diatoms. However, differences in utilization existed between stations outside and under the influence of the TPD surface current. At stations outside the TPD influence, specifically in the Nansen Basin, the lowest surface water [DSi] were associated with the sea-ice edge where light is more abundant and conditions are favorable for phytoplankton growth. Outside the TPD influence, DSi and Fe limitation determined the fate of phytoplankton blooms. Fe

limitation most likely caused the greater depletion of DSi compared to NO_3^- due to the associated increase in the Si:NO_3^- uptake ratio by diatoms. Significantly higher [DSi] and similar δ^{30}Si-DSi in the CAO are ascribed to the influence of the TPD surface current supplying nutrient-rich waters from the Siberian shelves. In waters under the TPD influence, despite the low Chl *a* and $bSiO_2$, depletion in [DSi] is observed, matching high δ^{30}Si-DSi in the surface waters (~10 m water depth), indicating the presence of diatoms (likely sea ice attached diatoms such as *M. arctica*). At these stations, low light availability and NO_3^- limitation are the major factors for the lower diatom production compared to outside the TPD influence, since generally high [DSi] and high [Fe] are maintained by river input and transport within the TPD. The deeper water column (~50 m water depth) inside the TPD showed increased [DSi] and decreased δ^{30}Si-DSi without indication for significant remineralization of $bSiO_2$. This suggests advection of shelf-derived waters with high river imprint rich in DSi and low in δ^{30}Si-DSi. Such conditions might change in a not so distant future due to climate change.

The use of open and closed system models usually helps to characterize the fractionation between seawater and diatoms during DSi uptake. In both areas, both models could not be validated. The complexity of the Arctic Ocean, with its low primary production, low nutrient concentration (outside the TPD influence), light limitation, and sea ice presence, along with the limited dataset presented here (few data points in shallow depths, where primary production is present, and late season sampling after the main bloom period), all contribute to the discrepancy between idealized models and the real ocean conditions. Additionally, the unknown influence of sea ice diatoms, which can be exported to the water column and have a higher δ^{30}Si-$bSiO_2$ (Fripiat et al., 2007), on δ^{30}Si-DSi in the Arctic Ocean complicates the interpretation of the isotope systematics (Varela et al., 2016). Furthermore, lack of information about modification of endmember water masses due to primary production and mixing over the shelf limits the definition of source waters necessary for the models. However, based on the local environmental conditions, the area outside the TPD most likely resembles an open or a semi-closed system due to the AW influence and melting of sea ice resupplying nutrients. Under the TPD, the area most likely resembles a semi closed system, where a parcel of water rich in nutrients is transported laterally from the shelf towards the CAO and further downward/upward mixing is reduced preventing replenishment of nutrients. Yet, future studies about Si cycle systematics in the surface Arctic Ocean should not only consider DSi comsumption by diatoms, but should also include an in depth investigation of additional processes influencing the distribution of Si isotopes in this area, specifically those occurring on the shelves.

Data Availability Statement

Dissolved and biogenic silicon isotope composition data included in this paper are available on PANGAEA database (https://doi.org/10.1594/PANGAEA.920105).

Acknowledgments
We thank the Captain and crew of R/V *Polarstern* for their help during expedition PS94. We further thank Martina Schulz, Phillip Böning and Christiane Lorenzen for the technical support and help in the laboratory. We thank Ronja Paffrath, Ole Valk, Imke Petersen and Franz Schröter for sampling. We thank Ursula Schauer and Michiel Rutgers van der Loeff as chief scientist and as GEOTRACES main PI (coordinator of the GEOTRACES part of the cruise), respectively. Finally, we would like to thank Damien Cardinal and the two anonymous reviewers for their critical reading, thoughtful comments and efforts toward improving our manuscript. This work was funded by the Deutsche Forschungsgemeinschaft (DFG) grant EH 484/2-1, project number 399076022. Conselho Nacional de Desenvolvimento Científico e Tecnológico (CNPq–Brazil) supported financially B.T.P.L as part of the Science without Borders Program with a PhD scholarship (grant 205644/2014-7). Open access funding enabled and organized by Projekt DEAL.

References

Aagaard, K. (1989). A synthesis of the Arctic Ocean circulation. *Rapports et procès-verbaux des reunions. International Council for the Exploration of the Sea*, *188*, 11–22.

Ardyna, M., Babin, M., Gosselin, M., Devred, E., Rainville, L., & Tremblay, J. É. (2014). Recent Arctic Ocean sea ice loss triggers novel fall phytoplankton blooms. *Geophysical Research Letters*, *41*, 6207–6212. https://doi.org/10.1002/2014gl061047

Arrigo, K. R. (2017). Sea ice as a habitat for primary producers. In D. N. Thomas (Ed.), *Sea Ice* (3rd ed., pp. 352–369). John Wiley & Sons, Ltd. https://doi.org/10.1002/9781118778371.ch14

Arrigo, K. R., Mock, T., & Lizotte, M. P., (2010). Primary producers in sea ice. In D. N. Thomas, & G. S. Dieckman (Eds.), *Sea Ice* (2nd ed., pp. 283–326). Blackwell Publishing Ltd. https://doi.org/10.1002/9781444317145.ch8

Arrigo, K. R., Perovich, D. K., Pickart, R. S., Brown, Z. W., van Dijken, G. L., Lowry, K. E., et al. (2012). Massive phytoplankton blooms under arctic sea ice. *Science*, *336*, 1408–1408. https://doi.org/10.1126/science.1215065

Arrigo, K. R., van Dijken, G., & Pabi, S. (2008). Impact of a shrinking Arctic ice cover on marine primary production. *Geophysical Research Letters*, *35*, 1–6. https://doi.org/10.1029/2008gl035028

Arrigo, K. R., & van Dijken, G. L. (2015). Continued increases in Arctic Ocean primary production. *Progress in Oceanography*, *136*, 60–70. https://doi.org/10.1016/j.pocean.2015.05.002

Assmy, P., Fernández-Méndez, M., Duarte, P., Meyer, A., Randelhoff, A., Mundy, C. J., et al. (2017). Leads in Arctic pack ice enable early phytoplankton blooms below snow-covered sea ice. *Scientific Reports*, *7*, 40850. https://doi.org/10.1038/srep40850

Bodungen, B. V., Wunsch, M., & Fürderer, H. (1991). Sampling and analysis of suspended and sinking particles in the Northern North Atlantic. In D. C. Hurd & D. W. Spencer (Eds.), *Marine Particles: Analysis and Characterization* (Vol. *63*, pp. 47–56). American Geophysical Union (AGU). https://doi.org/10.1029/GM063p0047

Boetius, A., Albrecht, S., Bakker, K., Bienhold, C., Felden, J., Fernández-Méndez, M., et al. (2013). Export of algal biomass from the melting Arctic sea ice. *Science*, *339*, 1430–1432. https://doi.org/10.1126/science.1231346

Brzezinski, M. A. (1985). The Si: C: N ratio of marine diatoms: Interspecific variability and the effect of some environmental variables. *Journal of Phycology*, *21*, 347–357. https://doi.org/10.1111/j.0022-3646.1985.00347.x

Brzezinski, M. A., Closset, I., Jones, J. L., de Souza, G. F., & Maden, C. (2021). New constraints on the physical and biological controls on the silicon isotopic composition of the Arctic Ocean. *Frontiers in Marine Science*, *8*, 699762. https://doi.org/10.3389/fmars.2021.699762

Brzezinski, M. A., Dickson, M. L., Nelson, D. M., & Sambrotto, R. (2003). Ratios of Si, C and N uptake by microplankton in the Southern Ocean. *Deep Sea Research Part II: Topical Studies in Oceanography*, *50*, 619–633. https://doi.org/10.1016/s0967-0645(02)00587-8

Brzezinski, M. A., & Jones, J. L. (2015). Coupling of the distribution of silicon isotopes to the meridional overturning circulation of the North Atlantic Ocean. *Deep Sea Research Part II: Topical Studies in Oceanography*, *116*, 79–88. https://doi.org/10.1016/j.dsr2.2014.11.015

Cardinal, D., Alleman, L. Y., Dehairs, F., Savoye, N., Trull, T. W., & André, L. (2005). Relevance of silicon isotopes to Si-nutrient utilization and Si-source assessment in Antarctic waters. *Global Biogeochemical Cycles*, *19*, 1–13. https://doi.org/10.1029/2004gb002364

Cardinal, D., Alleman, L. Y., de Jong, J., Ziegler, K., & André, L. (2003). Isotopic composition of silicon measured by multicollector plasma source mass spectrometry in dry plasma mode. *Journal of Analytical Atomic Spectrometry*, *18*, 213–218. https://doi.org/10.1039/b210109b

Charette, M. A., Kipp, L. E., Jensen, L. T., Dabrowski, J. S., Whitmore, L. M., Fitzsimmons, J. N., et al. (2020). The transpolar drift as a source of riverine and shelf-derived trace elements to the Central Arctic Ocean. *Journal of Geophysical Research: Oceans*, *125*, e2019JC015920. https://doi.org/10.1029/2019JC015920

Claquin, P., Martin-Jézéquel, V., Kromkamp, J. C., Veldhuis, M. J. W., & Kraay, G. W. (2002). Uncoupling of silicon compared with carbon and nitrogen metabolisms and the role of the cell cycle in continuous cultures of Thalassiosira pseudonana (Bacillariophyceae) under light, nitrogen, and phosphorus control. *Journal of Phycology*, *38*, 922–930. https://doi.org/10.1046/j.1529-8817.2002.t01-1-01220.x

Codispoti, L. A., Friederich, G. E., Sakamoto, C. M., & Gordon, L. I. (1991). Nutrient cycling and primary production in the marine systems of the Arctic and Antarctic. *Journal of Marine Systems*, *2*, 359–384. https://doi.org/10.1016/0924-7963(91)90042-s

De La Rocha, C. (2002). Measurement of silicon stable isotope natural abundances via multicollector inductively coupled plasma mass spectrometry (MC-ICP-MS). *Geochemistry, Geophysics, Geosystems*, *3*, 1–8. https://doi.org/10.1029/2002gc000310

De La Rocha, C., Brzezinski, M. A., & DeNiro, M. J. (1997). Fractionation of silicon isotopes by marine diatoms during biogenic silica formation. *Geochimica et Cosmochimica Acta*, *61*, 5051–5056. https://doi.org/10.1016/s0016-7037(97)00300-1

De La Rocha, C., Brzezinski, M. A., & DeNiro, M. J. (2000). A first look at the distribution of the stable isotopes of silicon in natural waters. *Geochimica et Cosmochimica Acta*, *64*, 2467–2477. https://doi.org/10.1016/s0016-7037(00)00373-2

De La Rocha, C. L., Brzezinski, M. A., DeNiro, M. J., & Shemesh, A. (1998). Silicon-isotope composition of diatoms as an indicator of past oceanic change. *Nature*, *395*, 680–683. https://doi.org/10.1038/27174

Demarest, M. S., Brzezinski, M. A., & Beucher, C. P. (2009). Fractionation of silicon isotopes during biogenic silica dissolution. *Geochimica et Cosmochimica Acta*, *73*, 5572–5583. https://doi.org/10.1016/j.gca.2009.06.019

de Souza, G. F., Reynolds, B. C., Rickli, J., Frank, M., Saito, M. A., Gerringa, L. J., et al. (2012). Southern Ocean control of silicon stable isotope distribution in the deep Atlantic Ocean. *Global Biogeochemical Cycles*, *26*, GB2035. https://doi.org/10.1029/2011gb004141

Dittmar, T., & Kattner, G. (2003). The biogeochemistry of the river and shelf ecosystem of the Arctic Ocean: A review. *Marine Chemistry*, *83*, 103–120. https://doi.org/10.1016/s0304-4203(03)00105-1

Douthitt, C. (1982). The geochemistry of the stable isotopes of silicon. *Geochimica et Cosmochimica Acta*, *46*, 1449–1458. https://doi.org/10.1016/0016-7037(82)90278-2

Edler, L. (1979). *Phytoplankton and chlorophyll: Recommendations on methods for marine biological studies in the Baltic Sea* (Vol. *5*, pp. 1–38). Baltic Marine Biologists Publication.

Ehlert, C., Reckhardt, A., Greskowiak, J., Liguori, B. T. P., Böning, P., Paffrath, R., et al. (2016). Transformation of silicon in a sandy beach ecosystem: Insights from stable silicon isotopes from fresh and saline groundwaters. *Chemical Geology*, *440*, 207–218. https://doi.org/10.1016/j.chemgeo.2016.07.015

Engström, E. (2009). *Fractionation of the stable silicon isotopes studied using MC-ICPMS: Analytical method developments and applications in geochemistry. Doctoral thesis, Luleå University of Technology*. Retrieved from http://www.diva-portal.org/smash/get/diva2:991723/FULLTEXT01.pdf

Evans, J. R., & Anderson, J. M. (1987). Absolute absorption and relative fluorescence excitation spectra of the five major chlorophyll-protein complexes from spinach thylakoid membranes. *Bioenergetics*, *892*, 75–82. https://doi.org/10.1016/0005-2728(87)90249-0

Fernández-Méndez, M., Katlein, C., Rabe, B., Nicolaus, M., Peeken, I., Bakker, K., et al. (2015). Photosynthetic production in the central Arctic Ocean during the record sea-ice minimum in 2012. *Biogeosciences*, *12*, 3525–3549. https://doi.org/10.5194/bg-12-3525-2015

Fernández-Méndez, M., Wenzhöfer, F., Peeken, I., Sørensen, H. L., Glud, R. N., & Boetius, A. (2014). Composition, buoyancy regulation and fate of ice algal aggregates in the Central Arctic Ocean. *PLoS One*, *9*, e107452. https://doi.org/10.1371/journal.pone.0107452

Fripiat, F., Cardinal, D., Tison, J. L., Worby, A., & André, L. (2007). Diatom-induced silicon isotopic fractionation in Antarctic sea ice. *Journal of Geophysical Research: Biogeosciences*, *112*, G02001. https://doi.org/10.1029/2006jg000244

Georg, R. B., Reynolds, B. C., Frank, M., & Halliday, A. N. (2006). New sample preparation techniques for the determination of Si isotopic compositions using MC-ICPMS. *Chemical Geology*, *235*, 95–104. https://doi.org/10.1016/j.chemgeo.2006.06.006

Gosselin, M., Levasseur, M., Wheeler, P. A., Horner, R. A., & Booth, B. C. (1997). New measurements of phytoplankton and ice algal production in the Arctic Ocean. *Deep Sea Research Part II: Topical Studies in Oceanography*, *44*, 1623–1644. https://doi.org/10.1016/s0967-0645(97)00054-4

Grasse, P., Brzezinski, M. A., Cardinal, D., de Souza, G., Andersson, P., Closset, I., et al. (2017). GEOTRACES inter-calibration of the stable silicon isotope composition of dissolved silicic acid in seawater. *Journal of Analytical Atomic Spectrometry*, *32*, 562–578. https://doi.org/10.1039/c6ja00302h

Hansen, H. P., & Koroleff, F. (1999). Determination of nutrients. K. Grasshoff, K. Kremling & Manfred Ehrhardt (Eds.), *Methods of seawater analysis* (3rd ed., pp. 159–228). WILEY-VCH Verlag GmbH. https://doi.org/10.1002/9783527613984.ch10

Hátún, H., Azetsu-Scott, K., Somavilla, R., Rey, F., Johnson, C., Mathis, M., et al. (2017). The subpolar gyre regulates silicate concentrations in the North Atlantic. *Scientific Reports*, *7*, 14576. https://doi.org/10.1038/s41598-017-14837-4

IPCC. (2014). *Climate change 2014: Synthesis report. Contribution of working groups I, II and III to the fifth assessment report of the intergovernmental panel on climate change*.

Jones, E. P., Swift, J. H., Anderson, L. G., Lipizer, M., Civitarese, G., Falkner, K. K., et al. (2003). Tracing Pacific water in the North Atlantic Ocean. *Journal of Geophysical Research: Oceans*, *108*, 3116. https://doi.org/10.1029/2001jc001141

Karl, D. M., & Tien, G. (1992). MAGIC: A sensitive and precise method for measuring dissolved phosphorus in aquatic environments. *Limnology and Oceanography*, *37*, 105–116. https://doi.org/10.4319/lo.1992.37.1.0105

Kipp, L. E., Charette, M. A., Moore, W. S., Henderson, P. B., & Rigor, I. G. (2018). Increased fluxes of shelf-derived materials to the central Arctic Ocean. *Science Advances*, *4*, eaao1302. https://doi.org/10.1126/sciadv.aao1302
Krumpen, T., Belter, H. J., Boetius, A., Damm, E., Haas, C., Hendricks, S., et al. (2019). Arctic warming interrupts the Transpolar Drift and affects long-range transport of sea ice and ice-rafted matter. *Scientific Reports*, *9*, 5459. https://doi.org/10.1038/s41598-019-41456-y
Lalande, C., Nöthig, E. M., & Fortier, L. (2019). Algal export in the Arctic Ocean in times of global warming. *Geophysical Research Letters*, *46*, 5959–5967. https://doi.org/10.1029/2019gl083167
Lalande, C., Nöthig, E. M., Somavilla, R., Bauerfeind, E., Shevchenko, V., & Okolodkov, Y. (2014). Variability in under-ice export fluxes of biogenic matter in the Arctic Ocean. *Global Biogeochemical Cycles*, *28*, 571–583. https://doi.org/10.1002/2013gb004735
Laney, S. R., Krishfield, R. A., & Toole, J. M. (2017). The euphotic zone under Arctic Ocean sea ice: Vertical extents and seasonal trends. *Limnology and Oceanography*, *62*, 1910–1934. https://doi.org/10.1002/lno.10543
Leu, E., Søreide, J. E., Hessen, D. O., Falk-Petersen, S., & Berge, J. (2011). Consequences of changing sea-ice cover for primary and secondary producers in the European Arctic shelf seas: Timing, quantity, and quality. *Progress in Oceanography*, *90*, 18–32. https://doi.org/10.1016/j.pocean.2011.02.004
Lewis, K. M., Arntsen, A. E., Coupel, P., Joy-Warren, H., Lowry, K. E., Matsuoka, A., et al. (2019). Photoacclimation of Arctic Ocean phytoplankton to shifting light and nutrient limitation. *Limnology and Oceanography*, *64*, 284–301. https://doi.org/10.1002/lno.11039
Lewis, K. M., Van Dijken, G. L., & Arrigo, K. R. (2020). Changes in phytoplankton concentration now drive increased Arctic Ocean primary production. *Science*, *369*, 198–202. https://doi.org/10.1126/science.aay8380
Liguori, B. T. P., Ehlert, C., Nöthig, E.-M., van Ooijen, J. C., & Pahnke, K. (2020). Silicon isotopes in surface waters during POLARSTERN cruise PS94 ARK-XXIX/3) in 2015. *PANGAEA*. https://doi.org/10.1594/PANGAEA.920105
Liguori, B. T. P., Ehlert, C., & Pahnke, K. (2020). The influence of water mass mixing and particle dissolution on the silicon cycle in the Central Arctic Ocean. *Frontiers in Marine Science*, *7*, 202. https://doi.org/10.3389/fmars.2020.00202
Mavromatis, V., Rinder, T., Prokushkin, A. S., Pokrovsky, O. S., Korets, M. A., Chmeleff, J., et al. (2016). The effect of permafrost, vegetation, and lithology on Mg and Si isotope composition of the Yenisey River and its tributaries at the end of the spring flood. *Geochimica et Cosmochimica Acta*, *191*, 32–46. https://doi.org/10.1016/j.gca.2016.07.003
National Snow and Ice Data Center (2015). Retrieved from https://nsidc.org/arcticseaicenews/2015/10
Nelson, D. M., Tréguer, P., Brzezinski, M. A., Leynaert, A., & Quéguiner, B. (1995). Production and dissolution of biogenic silica in the ocean: Revised global estimates, comparison with regional data and relationship to biogenic sedimentation. *Global Biogeochemical Cycles*, *9*, 359–372. https://doi.org/10.1029/95gb01070
Nöthig, E.-M., Petersen, I., Schröter, F., & Lorenzen, C. (2018). Chlorophyll a measured on water bottle samples during POLARSTERN cruise PS94 (ARK-XXIX/3). *PANGAEA*. https://doi.org/10.1594/PANGAEA.887934
Nöthig, E.-M., Ramondenc, S., Haas, A., Hehemann, L., Walter, A., Bracher, A., et al. (2020). Summertime chlorophyll a and particulate organic carbon standing stocks in surface waters of the Fram Strait and the Arctic Ocean (1991 – 2015). *Frontiers in Marine Science*, *7*, 350. https://doi.org/10.3389/fmars.2020.00350
Nummelin, A., Ilicak, M., Li, C., & Smedsrud, L. H. (2016). Consequences of future increased Arctic runoff on Arctic Ocean stratification, circulation, and sea ice cover. *Journal of Geophysical Research: Oceans*, *121*, 617–637. https://doi.org/10.1002/2015jc011156
Oelze, M., Schuessler, J. A., & von Blanckenburg, F. (2016). Mass bias stabilization by Mg doping for Si stable isotope analysis by MC-ICP-MS. *Journal of Analytical Atomic Spectrometry*, *31*, 2094–2100. https://doi.org/10.1039/c6ja00218h
Paffrath, R., Laukert, G., Bauch, D., Rutgers van der Loeff, M., & Pahnke, K. (2021). Separating individual contributions of major Siberian rivers in the Transpolar Drift of the Arctic Ocean. *Scientific Reports*, *11*, 1–11. https://doi.org/10.1038/s41598-021-86948-y
Perovich, D. K. (2017). Sea ice and sunlight. In D. N. Thomas (Ed.), *Sea Ice* (3rd ed., pp. 110–137). John Wiley & Sons, Ltd. https://doi.org/10.1002/9781118778371.ch4
Peterson, B. J., Holmes, R. M., McClelland, J. W., Vörösmarty, C. J., Lammers, R. B., Shiklomanov, A. I., et al. (2002). Increasing river discharge to the Arctic Ocean. *Science*, *298*, 2171–2173. https://doi.org/10.1126/science.1077445
Pokrovsky, O. S., Reynolds, B. C., Prokushkin, A. S., Schott, J., & Viers, J. (2013). Silicon isotope variations in Central Siberian rivers during basalt weathering in permafrost-dominated larch forests. *Chemical Geology*, *355*, 103–116. https://doi.org/10.1016/j.chemgeo.2013.07.016
Polyakov, I. V., Pnyushkov, A. V., Alkire, M. B., Ashik, I. M., Baumann, T. M., Carmack, E. C., et al. (2017). Greater role for Atlantic inflows on sea-ice loss in the Eurasian Basin of the Arctic Ocean. *Science*, *356*, 285–291. https://doi.org/10.1126/science.aai8204
Pomeroy, L. R. (1997). Primary production in the Arctic Ocean estimated from dissolved oxygen. *Journal of Marine Systems*, *10*, 1–8. https://doi.org/10.1016/s0924-7963(96)00059-0
Poulin, M., Underwood, G. J., & Michel, C. (2014). Sub-ice colonial *Melosira arctica* in Arctic first-year ice. *Diatom Research*, *29*, 213–221. https://doi.org/10.1080/0269249x.2013.877085
Ragueneau, O. G., Savoye, N., Del Amo, Y., Cotten, J., Tardiveau, B., & Leynaert, A. (2005). A new method for the measurement of biogenic silica in suspended matter of coastal waters: Using Si:Al ratios to correct for the mineral interference. *Continental Shelf Research*, *25*, 697–710. https://doi.org/10.1016/j.csr.2004.09.017
Randelhoff, A., Sundfjord, A., & Reigstad, M. (2015). Seasonal variability and fluxes of nitrate in the surface waters over the Arctic shelf slope. *Geophysical Research Letters*, *42*, 3442–3449. https://doi.org/10.1002/2015gl063655
Reynolds, B. C., Aggarwal, J., Andre, L., Baxter, D., Beucher, C., Brzezinski, M. A., et al. (2007). An inter-laboratory comparison of Si isotope reference materials. *Journal of Analytical Atomic Spectrometry*, *22*, 561–568. https://doi.org/10.1039/b616755a
Reynolds, B. C., Frank, M., & Halliday, A. N. (2006). Silicon isotope fractionation during nutrient utilization in the North Pacific. *Earth and Planetary Science Letters*, *244*, 431–443. https://doi.org/10.1016/j.epsl.2006.02.002
Rijkenberg, M. J., Slagter, H. A., Rutgers van der Loeff, M., van Ooijen, J., & Gerringa, L. J. (2018). Dissolved Fe in the deep and upper Arctic Ocean with a focus on Fe limitation in the Nansen Basin. *Frontiers in Marine Science*, *5*, 88. https://doi.org/10.3389/fmars.2018.00088
Romero, O., & Hebbeln, D. (2003). Biogenic silica and diatom thanatocoenosis in surface sediments below the Peru-Chile Current: Controlling mechanisms and relationship with productivity of surface waters. *Marine Micropaleontology*, *48*, 71–90. https://doi.org/10.1016/s0377-8398(02)00161-5
Rudels, B. (2012). Arctic Ocean circulation and variability–advection and external forcing encounter constraints and local processes. *Ocean Science*, *8*, 261–286. https://doi.org/10.5194/os-8-261-2012
Rudels, B., Anderson, L. G., & Jones, E. P. (1996). Formation and evolution of the surface mixed layer and halocline of the Arctic Ocean. *Journal of Geophysical Research*, *101*, 8807–8821. https://doi.org/10.1029/96jc00143
Rudels, B., Jones, E. P., Schauer, U., & Eriksson, P. (2004). Atlantic sources of the Arctic Ocean surface and halocline waters. *Polar Research*, *23*, 181–208. https://doi.org/10.3402/polar.v23i2.6278

Rudels, B., Larsson, A. M., & Sehlstedt, P. I. (1991). Stratification and water mass formation in the Arctic Ocean: Some implications for the nutrient distribution. *Polar Research*, *10*, 19–32. https://doi.org/10.3402/polar.v10i1.6724

Rutgers van der Loeff, M., Kipp, L. E., Charette, M. A., Moore, W. S., Black, E., Stimac, I., et al. (2018). Radium isotopes across the Arctic Ocean show time scales of water mass ventilation and increasing shelf inputs. *Journal of Geophysical Research: Oceans*, *123*, 4853–4873. https://doi.org/10.1029/2018jc013888

Sarmiento, J. L., Gruber, N., Brzezinski, M. A., & Dunne, J. P. (2004). High-latitude controls of thermocline nutrients and low latitude biological productivity. *Nature*, *427*, 56–60. https://doi.org/10.1038/nature02127

Schauer, U. (2016). *The expedition PS94 of the research vessel POLARSTERN to the central Arctic Ocean in 2015. Reports on polar and marine research*. (Vol. *703*, pp. 1–170). Bremerhaven, Germany: Alfred-Wegener-Institut, Helmholtz-Zentrum für Polar- und Meeresforschung. https://doi.org/10.2312/BzPM_0703_2016

Schlitzer, R. (2018). Ocean data view. Retrieved from www.odv.awi.de

Schuur, E. A. G., & Mack, M. C. (2018). Ecological response to permafrost thaw and consequences for local and global ecosystem services. *Annual Review of Ecology, Evolution, and Systematics*, *49*, 279–301. https://doi.org/10.1146/annurev-ecolsys-121415-032349

Slagter, H. A., Reader, H. E., Rijkenberg, M. J. A., Rutgers Van Der Loeff, M., de Baar, H. J. W., & Gerringa, L. J. A. (2017). Organic Fe speciation in the Eurasian Basins of the Arctic Ocean and its relation to terrestrial DOM. *Marine Chemistry*, *197*, 11–25. https://doi.org/10.1016/j.marchem.2017.10.005

Stedmon, C. A., Amon, R. M. W., Rinehart, A. J., & Walker, S. A. (2011). The supply and characteristics of colored dissolved organic matter (CDOM) in the Arctic Ocean: Pan Arctic trends and differences. *Marine Chemistry*, *124*, 108–118. https://doi.org/10.1016/j.marchem.2010.12.007

Stroeve, J. C., Schroder, D., Tsamados, M., & Feltham, D. (2018). Warm winter, thin ice? *The Cryosphere*, *12*, 1791–1809. https://doi.org/10.5194/tc-12-1791-2018

Sun, X., Mörth, C. M., Porcelli, D., Kutscher, L., Hirst, C., Murphy, M. J., et al. (2018). Stable silicon isotopic compositions of the Lena River and its tributaries: Implications for silicon delivery to the Arctic Ocean. *Geochimica et Cosmochimica Acta*, *241*, 120–133. https://doi.org/10.1016/j.gca.2018.08.044

Sutton, J. N., de Souza, G. F., García-Ibáñez, M. I., & De La Rocha, C. L. (2018). The silicon stable isotope distribution along the GEOVIDE section (GEOTRACES GA-01) of the North Atlantic Ocean. *Biogeosciences*, *15*, 5663–5676. https://doi.org/10.5194/bg-15-5663-2018

Sutton, J. N., Varela, D. E., Brzezinski, M. A., & Beucher, C. P. (2013). Species-dependent silicon isotope fractionation by marine diatoms. *Geochimica et Cosmochimica Acta*, *104*, 300–309. https://doi.org/10.1016/j.gca.2012.10.057

Tréguer, P. J., & De La Rocha, C. L. (2013). The world ocean silica cycle. *Annual Review of Marine Science*, *5*, 477–501. https://doi.org/10.1146/annurev-marine-121211-172346

Tréguer, P. J., & Pondaven, P. (2000). Silica control of carbon dioxide. *Nature*, *406*, 358–359. https://doi.org/10.1038/35019236

Uhlig, C., Damm, E., Peeken, I., Krumpen, T., Rabe, B., Korhonen, M., et al. (2019). Sea ice and water mass influence dimethylsulfide concentrations in the central Arctic Ocean. *Frontiers in Earth Science*, *7*, 179. https://doi.org/10.3389/feart.2019.00179

van Ooijen, J. C., Rijkenberg, M. J. A., Gerringa, L. J. A., Rabe, B., & Rutgers van der Loeff, M. (2016). Inorganic nutrients measured on water bottle samples during Polarstern cruise PS94 (ARK-XXIX/3). *PANGAEA*. https://doi.org/10.1594/PANGAEA.868396

Varela, D. E., Brzezinski, M. A., Beucher, C. P., Jones, J. L., Giesbrecht, K. E., Lansard, B., et al. (2016). Heavy silicon isotopic composition of silicic acid and biogenic silica in Arctic waters over the Beaufort shelf and the Canada Basin. *Global Biogeochemical Cycles*, *30*, 804–824. https://doi.org/10.1002/2015gb005277

Varela, D. E., Pride, C. J., & Brzezinski, M. A. (2004). Biological fractionation of silicon isotopes in Southern Ocean surface waters. *Global Biogeochemical Cycles*, *18*, GB1047. https://doi.org/10.1029/2003gb002140

Wassmann, P., & Reigstad, M. (2011). Future Arctic Ocean seasonal ice zones and implications for pelagic-benthic coupling. *Oceanography*, *24*, 220–231. https://doi.org/10.5670/oceanog.2011.74

Woodgate, R. A. (2018). Increases in the Pacific inflow to the Arctic from 1990 to 2015, and insights into seasonal trends and driving mechanisms from year-round Bering Strait mooring data. *Progress in Oceanography*, *160*, 124–154. https://doi.org/10.1016/j.pocean.2017.12.007

Zernova, V., Nöthig, E.-M., & Shevchenko, V. (2000). Vertical microalga flux in the northern Laptev Sea (From the data collected by the yearlong sediment trap). *Oceanology*, *40*, 801–808.

Zhang, X., Walsh, J. E., Zhang, J., Bhatt, U. S., & Ikeda, M. (2004). Climatology and interannual variability of Arctic cyclone activity: 1948–2002. *Journal of Climate*, *17*, 2300–2317. https://doi.org/10.1175/1520-0442(2004)017<2300:caivoa>2.0.co;2

References From the Supporting Information

Bauch, D., Rutgers van der Loeff, M., Andersen, N., Torres-Valdes, S., Bakker, K., & Abrahamsen, E. P. (2011). Origin of freshwater and polynya water in the Arctic Ocean halocline in summer 2007. *Progress in Oceanography*, *91*, 482–495. https://doi.org/10.1016/j.pocean.2011.07.017

Newton, R., Schlosser, P., Mortlock, R., Swift, J., & MacDonald, R. (2013). Canadian Basin freshwater sources and changes: Results from the 2005 Arctic Ocean Section. *Journal of Geophysical Research: Oceans*, *118*, 2133–2154. https://doi.org/10.1002/jgrc.20101